A LOW-SPEED WIND TUNNEL STUDY OF VORTEX INTERACTION CONTROL TECHNIQUES ON A CHINE-FOREBODY/DELTA-WING CONFIGURATION

By Dhanvada M. Rao and M.K. Bhat
VíGYAN, Inc., Hampton, VA

ABSTRACT

A low-speed wind tunnel evaluation was conducted of passive and active techniques proposed as a means to impede the interaction of forebody chine and delta wing vortices, when such interaction leads to undesirable aerodynamic characteristics particularly in the post-stall regime. The passive method was based on physically disconnecting the chine/wing junction; the active technique employed deflection of inboard leading edge flaps. In either case, the intent was to forcibly shed the chine vortices before they encountered the downwash of wing vortices. Flow visualizations, wing pressures and six-component force/moment measurements confirmed the benefits of forced vortex de-coupling at post-stall angles of attack and in sideslip, viz., alleviation of post-stall zero-beta asymmetry, lateral instability and twin-tail buffet, with insignificant loss of maximum lift.

NOMENCLATURE

C_L	Lift coefficient
C_l	Rolling moment coefficient
C_m	Pitching moment coefficient
C_n	Yawing moment coefficient
$C_{p,u}$	Wing upper-surface static pressure coefficient
DC	Time-averaged voltage output of vertical tail strain-gage bridge
R.M.S.	Root-mean-square of voltage output of vertical tail strain-gage bridge
S	Wing semi-span
Y	Coordinate parallel to wing span
Z	Coordinate normal to wing plane
α	Angle of attack
ß	Angle of sideslip

INTRODUCTION

Chined forebodies closely coupled with thin, highly-swept wings are of particular interest in relation to supersonic tactical aircraft configured for high maneuverability. The favorable interaction of chine and leading edge vortices delays vortex breakdown to higher angles of attack, thus improving the maximum lift and lateral/directional stability characteristics. In the post-stall region however, abrupt and non-symmetrical breakdown of the interacting vortices leads to pronounced pitch-up, lateral sensitivity, hysteresis and tail buffet problems (refs. 1-3). An opportunity therefore exists for the application of innovative vortex management techniques as means to alleviate the high-alpha limitations of coupled chine-wing configurations and enhance the post-stall maneuver potential. It was considered worth exploring the feasibility of selective de-coupling of the chine and wing vortices above critical angles of attack and side-slip, in order to delay the onset of uncontrollable and potentially hazardous aerodynamic asymmetries.

The present study was directed towards evaluating (i) a simple geometrical modification of the chine/wing junction and (ii) inboard leading-edge flaps, as two alternate proposed approaches for the practical realization of vortex de-coupling concept. Low-speed wind tunnel investigations were performed of these two techniques on generic chine forebody/delta wing models. In the initial phase (briefly reported in ref. 4), smoke visualizations of the vortex interactions and de-coupling were conducted, and the resulting upper-surface pressure distributions measured across a spanwise section of the wing. This was followed by six-component force/moment tests on a geometrically

similar model which also incorporated buffet-gaged vertical tails.

CONCEPT DESCRIPTIONS

The vortex de-coupling techniques may be generically classified as passive (i.e., involving a fixed geometric modification of the coupled chines), or active (i.e., reversible movement or deployment of an aerodynamic surface). The present study included one example of each, viz., a 'de-coupled' chine and inboard leading edge flaps, schematically exhibited in fig. 1.

The 'de-coupled' chine is obtained by removing a relatively small area (i.e., in the order of 1 percent of total reference lifting area) of the chine at the wing apex junction. This seemingly minor but crucial modification is intended to force the chine vortices to shed along an elevated trajectory, thus escaping 'capture' by the intense downwash between the wing apex vortices to avoid incipient coupling of the chine/wing vortex systems. Although some lift penalty at moderate angles of attack might occur on account of vortex de-coupling, this may be an acceptable trade-off in return for significantly improved post-stall stability and control characteristics.

The purpose of inboard leading edge flaps is to suppress or reduce the wing apex vortices and thus the downwash between them. Flap deflection also creates a physical break at the chine/apex junction, promoting the shedding of chine vortices into a region of reduced downwash. The flap deflection may be programmed to initiate at a critical angle of attack; it may also be differentially applied when an aerodynamic asymmetry exists, e.g., in side-slip.

EXPERIMENTAL DETAILS

Flow Visualization and Pressure Model (fig. 2): The test configuration was composed of a 60 deg. flat plate delta wing, having sharp beveled leading and trailing edges, mounted in a mid-wing position. The ogive forebody of the cylindrical fuselage incorporated a flat-plate chine in the wing plane. Smoke injection slots were provided in the hollow forebody below the chines, and also at the wing leading edges. The wings were fitted with deflectable leading edge flaps covering the inboard 50 percent of exposed semi-span. A single row of upper-surface static pressure taps was installed in the wing panels at a spanwise section passing through the wing centroid. The pressure leads were connected to an external Scani-Valve system.

Force/Moment Model (fig. 3): This was geometrically similar to the first model with the addition of vertical tails. Two alternate tail arrangements, viz., a central and a twin-tail, were tested. The right member of the twin-tails was instrumented with root-bending moment strain gages (oriented for maximum sensitivity to the first-order bending mode), to indicate buffet onset and also to provide a measure of the steady-state tail side force. A six-component strain gage balance housed within the fuselage measured the overall force/moment characteristics. This model had replaceable leading edge flap segments to investigate the flap-span effect on vortex de-coupling.

The tests were performed in VíGYAN 3x4 ft. atmospheric, low-speed facility operated as a free-jet tunnel, covering angle of attack range of 0° to 50°, and side-slip angles between -20° and 20°. The pressure, balance and tail load data were acquired at a free-stream dynamic pressure of 10 pounds/sq. ft., the corresponding Reynolds number being approx. 0.4 million based on mean aerodynamic chord. The very low velocities (approximately 1 ft/sec. giving a Reynolds number of 6500) desirable for smoke visualizations were obtained by means of a low-power fan temporarily installed in the wind tunnel diffuser.

RESULTS AND DISCUSSION

Flow Visualizations

a) Baseline Chines: Smoke visualization photographs, obtained with the bellmouth-located camera and shown in fig. 4 provide an overview of the baseline chine and wing vortex trajectories, and their mutual interaction with increasing angle of attack. The pertinent observations are as follows:

   α = 10°: the chine and wing vortex pairs remain

distinct and non-interacting over the entire length of the wing;

α = 15° : the chine vortices begin to migrate towards the wing vortices, while the latter grow in size;

α = 20° : the chine vortices disappear underneath the wing vortices which are now bursting asymmetrically over the two wing panels;

α = 30° : total vortex breakdown on the wings.

The effect of increasing angle of side-slip at a constant α = 30°, is depicted in the photographs of fig. 5. They reveal:

ß = 5° : the windward wing is fully stalled; the leeward chine and wing vortex cores remain distinct but inter-twined.

ß = 10° : the stalled flow from the windward wing drifts leeward across the fuselage; the inter-twined leeward vortices begin to unravel;

ß = 15° and 20° : the leeward vortices continue to unravel and eventually de-couple.

The above-noted trends relating to chine/wing vortex interactions with increasing α and ß are broadly in agreement with the observations reported by previous researchers (e.g., ref. 2). In the context of post-stall behavior, the following characteristics are noteworthy:

a) asymmetrical breakdown of the interacting vortices at ß=0° which can initiate wing rock and roll departure, and

b) coherent vortex structure on the leeward wing while the windward panel is stalled, leading to roll instability.

Reduction of the above undesirable attributes of the coupled chine/wing configuration was adopted as a measure of vortex de-coupling effectiveness in the present investigations.

b) De-Coupled Chines: Light-sheet flow visualizations in a spanwise wing section with increasing angle of attack are presented in fig. 6, which compares the baseline and de-coupled chine configurations. These results graphically illustrate the capability of a seemingly minor chine modification in interfering with the natural vortex coupling phenomenon. A direct consequence of vortex de-coupling is the avoidance of high-alpha asymmetry generated by the coupled configuration (e.g., α=25° in fig. 6).

The effect of side-slip angle at a constant α=30° on the leeward vortex patterns (traced from the light-sheet visualizations) is shown in fig. 7. The chine and wing vortices in the case of de-coupled chines are seen to remain well apart throughout the range ß=5° to 20° (fig. 8). The implied reduction of vortex lift on the leeward wing due to vortex de-coupling will tend to relieve the post-stall roll instability of the baseline configuration.

c) Leading Edge Flaps: Light-sheet visualization photographs, at ß=0° and increasing angle of attack, with 30° down-deflected inboard leading-edge flaps are presented in fig. 9. The chine vortices are seen to remain coherent with no evident tendency to migrate towards the leading edges, suggesting a total de-coupling from the wing flow-field. In the visualization plane, located only a short distance behind the flaps, the leading edge vortices remain small up to α=25°,

and appear to be on the verge of breakdown at $\alpha=30°$; nevertheless the chine vortices show no sign of merging with the wing vortical regions. The vortex patterns at side- slip (traced from light-sheet visualizations) are shown in fig. 10. Comparison with fig. 7 shows the leading edge flaps to be at least as effective as de-coupled chines in impeding chine/wing vortex interaction.

Pressure Measurements

Mainly intended to corroborate the qualitative flow visualizations, wing upper-surface pressure measurements were also helpful in providing a preliminary quantification of the chine-wing vortex interaction effects. The pressure data are particularly informative with regard to the local lift and rolling moment trends associated with artificially de-coupled vortices when approaching stall and in the post-stall region, including the effects of side-slip.

Spanwise suction pressure distributions (on the wing pressure station shown in fig. 2) with increasing α and at $ß=0°$ are presented in fig. 11 (A) and 11 (B), which compare three forebody configurations, (viz., no chine, coupled chines and de-coupled chines). Noteworthy are the pronounced suction peaks on the coupled configuration ($\alpha=15°$ and 20°) as well as their asymmetrical collapse ($\alpha=25°$). These well-known vortical characteristics of the coupled chine configuration are conspicuously absent in the case of de-coupled chines. Generally, the suction pressure distributions in the de-coupled case remain symmetrical throughout the alpha range; they also suggest that although some lift loss might occur at moderate angles of attack due to vortex de-coupling, the maximum lift characteristics will probably not be significantly penalized.

The results with increasing ß at a constant $\alpha=30°$, shown in fig. 12, compare the coupled and de-coupled chines. A pronounced reduction of the suction peak on the left (i.e., leeward) wing panel at $ß=5°$; simultaneously with increased average suction level on the stalled windward panel are the noteworthy effects of de-coupling, which persist at higher side-slip angles. These results suggest that vortex de-coupling has potential for alleviating the high-alpha rolling moment instability of the coupled configuration, the windward and leeward wing panels both contributing favorably.

Pressure distributions at $\alpha=30°$ and $ß=5°$ comparing the de-coupled chines and 30° leading-edge flaps with the baseline configuration are shown in fig. 13. In the case of leading edge flaps, a suction peak appearing on the lee-side wing indicates a leading edge vortex starting outboard of the flap; however, the averaged lift of the leeward panel is reduced. Once again, the windward upper-surface suctions are seen to be augmented, just as in the case of de-coupled chines. A bar-chart comparison (included in fig. 13) of the sectional rolling moment (from suction - pressure integrations) indicates both the de-coupled chines and leading edge flaps to be equally effective in reducing the lateral instability of the coupled configuration.

Six-Component Force/Moment Measurements

The longitudinal ($ß=0°$) and lateral/directional ($ß=\pm5°$) results of the coupled configuration are shown in fig. 14. These data reveal a rapid onset of lateral and directional instability as the $C_{L,max}$ angle of attack ($\alpha=35°$) is approached. The results of a ß-sweep at $\alpha=30°$ (fig. 15) further show a pronounced increment of roll instability in the region $ß = \pm 3°$ to $\pm 4°$, which presages extreme lateral sensitivity and potential for roll departure.

A comparison of the side-slip characteristics of de-coupled chines relative to baseline (fig. 16) shows that, in the range $-5°<ß<5°$, the lift coefficient remains relatively constant, and both the directional and lateral stability are improved. A sharp change in the aerodynamic coefficients occurring at $ß = \pm 5°$ indicates a rapid collapse of the de-coupled flow field on the wing. The leading edge flaps, on the other hand, yield positive directional and lateral stability in the range $-5°< ß < 5°$, and continue to be well-behaved outside this side-slip range (fig. 17). A pronounced

pitch-down trend due to leading edge flap deflection is favorable for recovery from high-alpha maneuvers.

Yawing and rolling moment characteristics versus angle of attack at $\beta = 5°$, indicating the influence of flap span and deflection angle, are presented in figs. 18 and 19. Increasing flap span (at a constant 45° deflection) progressively improves the roll instability in the range $\alpha = 25°$ to 45° and, to a lesser degree, the post-stall yaw instability (fig. 18). This suggests that vortex de-coupling as well as wing flow improvement are operative. The flap angle is found to be somewhat less critical, the stability characteristics being relatively little affected in the range 30° to 60° flap deflection as shown in fig. 19.

Twin-Tail Load Characteristics

Steady-state (i.e., time averaged) and root-mean-square characteristics of vertical tail root bending moment gage output versus angle of attack respectively indicate the static and dynamic flow environment encountered by the wing-mounted tails. On the baseline configuration (fig. 20), the tail side-force initially acts inwards but reverses direction with increasing alpha. A plausible explanation for the side-force reversal is based on flow visualizations (see sketches accompanying fig. 20): at low alpha the un-coupled chine vortices passing between the tails induce a suction on their inside surfaces; at higher alpha, coupling with the wing vortices moves the vortex suction outboard of the tails thus reversing the side force. The outward-directed tail side-force peaks at about $\alpha = 25°$, which coincides with a steep rise in r.m.s indicative of vortex breakdown. The de-coupled chines reduce the outward side-force and also tend to moderate the tail r.m.s at post-stall angles of attack. The r.m.s reduction with leading edge flaps (fig. 21) suggest a particularly effective buffet alleviation capability.

CONCLUSIONS

The post-stall stability and control difficulties attributable to vortex interactions on closely-coupled chine/delta wing configurations, motivated a feasibility investigation of controlled vortex de-coupling using passive and active techniques. A low-speed wind tunnel study of de-coupled chines and leading-edge flaps on a generic flat-plate chine / 60 deg. delta wing configuration, including flow visualizations, wing pressure measurements and six-component force/moment tests, leads to the following main conclusions:

1. Chine/wing vortex de-coupling in the post-stall regime is feasible, using a passive chine modification or inboard leading edge flaps.

2. Vortex de-coupling significantly influences the wing suction-pressure characteristics leading to improved high-alpha aerodynamics of chine/wing configurations, viz., alleviation of zero-beta asymmetry and longitudinal and post-stall lateral instability.

3. The leading-edge flap apparently combines the benefits of vortex de-coupling and wing flow improvement. With the added capability of differential operation (yet to be explored), it promises to be a highly effective high-alpha manipulator.

4. Vortex de-coupling and improved post-stall wing flow environment provided by the leading-edge flaps will also have potential to alleviate twin-tail excitation.

While the results of this exploratory study have provided an experimental foundation for the vortex de-coupling concept and also demonstrated its potential benefits to the high-alpha aerodynamics of chine/wing configurations, they are subject to the limitations of a relatively low test Reynolds Number as well as simplified geometry (viz., flat plate non-blended chines and, unrepresentative wing sections). Follow-up tests are planned to overcome these configurational restrictions and also to address Mach and Reynolds Number effects, concentrating on the leading-edge flap as the preferred vortex manipulator concept.

ACKNOWLEDGEMENTS

This investigation was supported by NASA Langley Research Center under SBIR Contract No. NAS1 - 18856. The encouragement and interest shown by Dr. R.M. Hall and Mr. Gary E. Erickson of the Transonic Aerodynamics Branch are gratefully acknowledged.

REFERENCES

1. Carr, D.C.; and Gilbert, W.C.: Effects of Fuselage Forebody Geometry on Low-Speed Lateral Directional Characteristics of Twin-Tail Fighter Model at High Angles of Attack. NASA TP-1592, 1979.

2. Erickson, G.E.; and Brandon, J.M.: Low-speed Experimental Study of the Vortex Flow Effects of a Fighter Forebody Having Unconventional Cross-Section. AIAA Paper 85-1798-CP, 1985.

3. Hall, R.M; and Del Frate, J.H.: Interaction Between Forebody and Wing vortices, A Water Tunnel Study. AFWAL-TM-85-252, 1986.

4. Rao, D.M.: Feasibility study of Vortex Interaction Control on a chine Forebody/Delta Wing Configuration at High Angles of Attack. AIAA Atmospheric Flight Mechanics Conf., 1989. pp. 36-42.

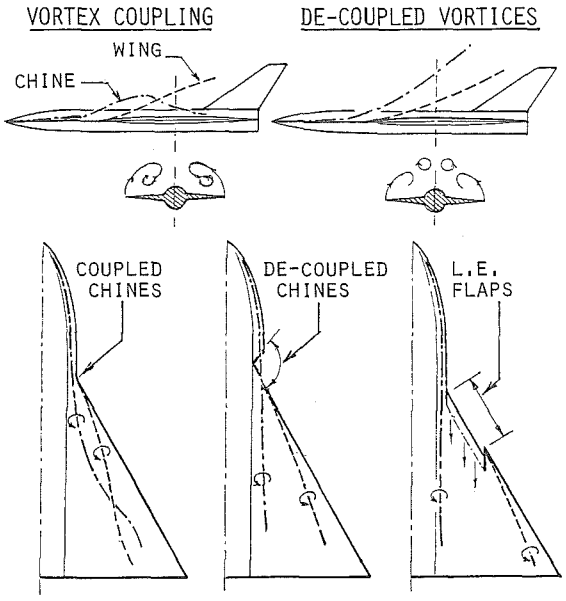

Fig. 1 Chine/wing vortex de-coupling concepts.

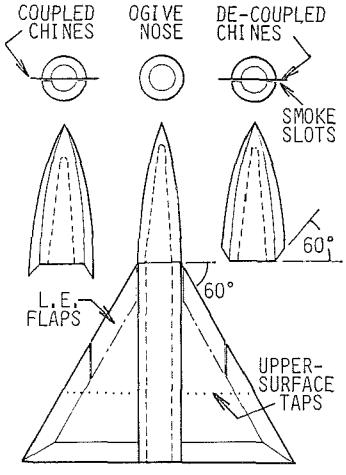

Fig. 2 Flow visualization and pressure model for vortex de-coupling tests.

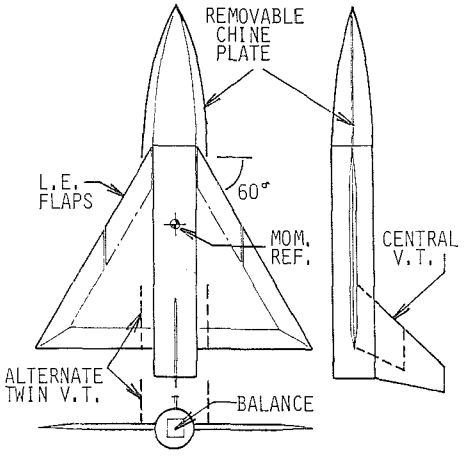

Fig. 3 Six-component force/moment for vortex de-coupling tests.

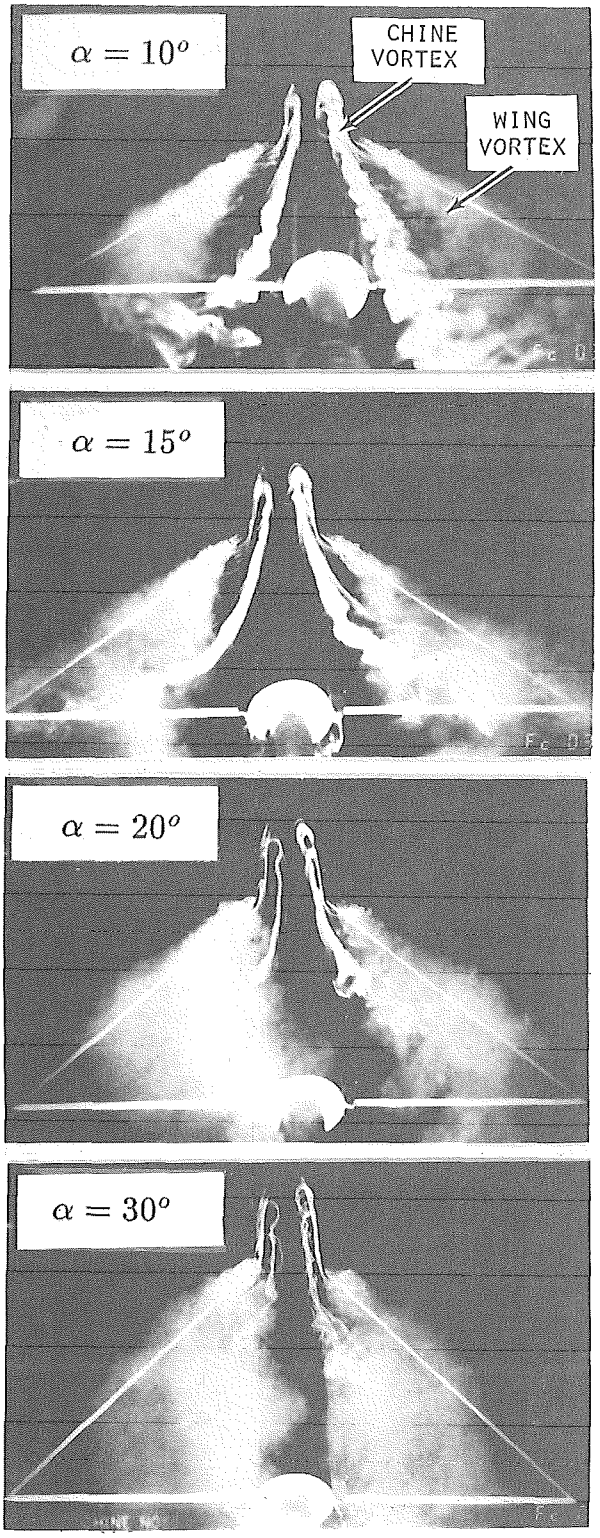

Fig. 4 Vortex patterns on coupled-chine configuration with increasing alpha.

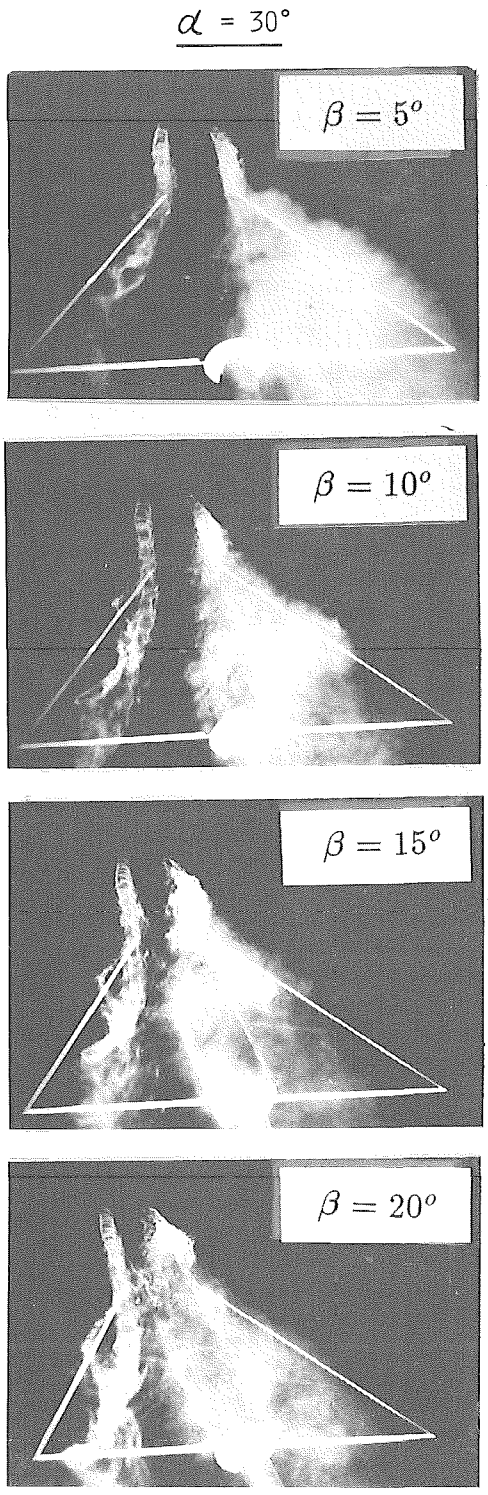

Fig. 5 Vortex patterns on coupled-chine configuration with increasing side-slip.

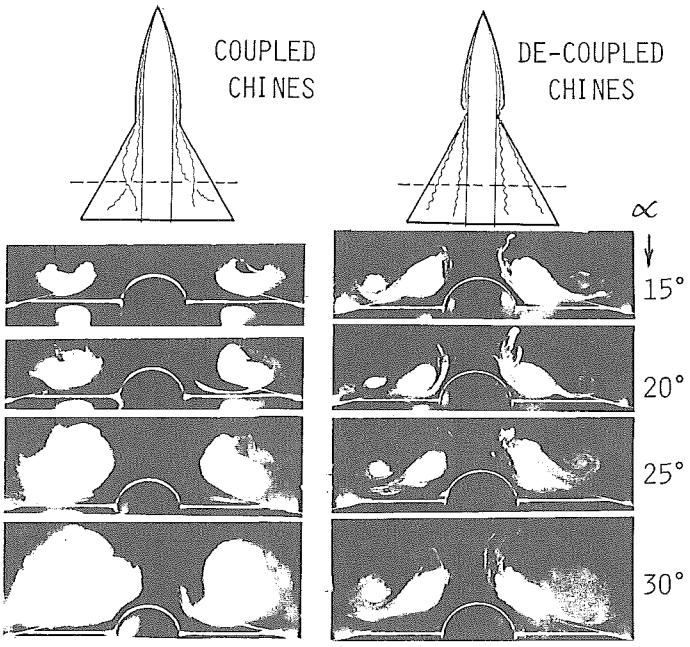

Fig. 6 Vortex patterns in wing cross-flow plane with increasing alpha: coupled versus de-coupled chines.

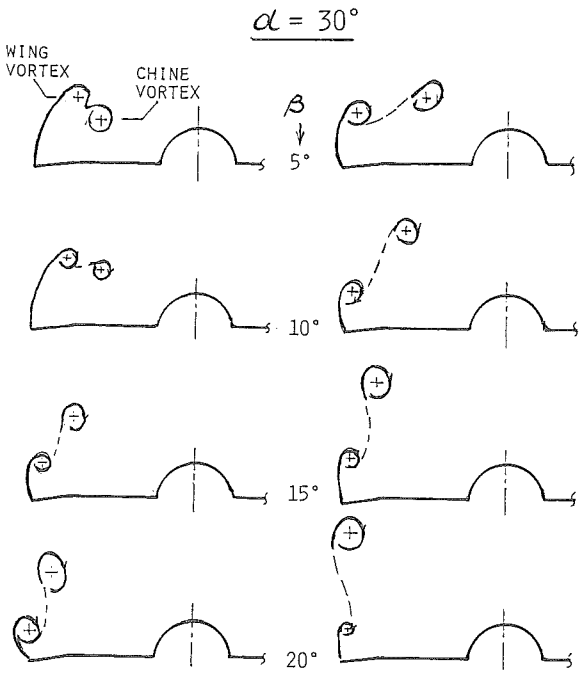

Fig. 7 Leeward vortex patterns in wing cross-plane with increasing side-slip; coupled versus de-coupled chines.

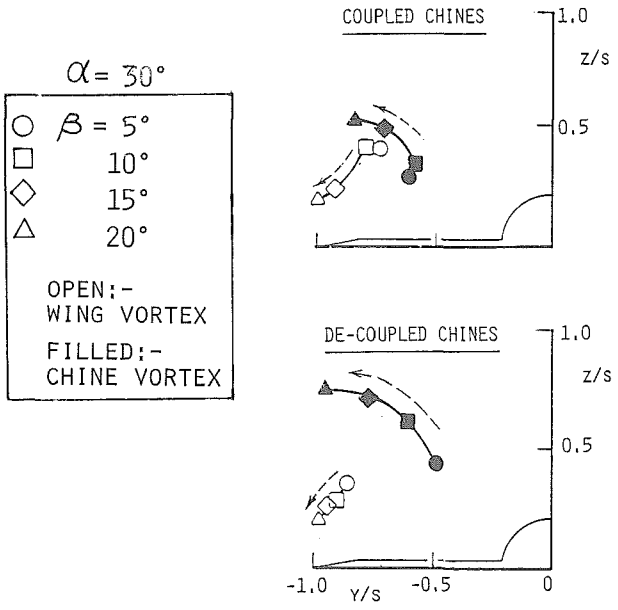

Fig. 8 Leeward vortex positions in wing cross-plane with increasing side-slip; coupled versus de-coupled chines.

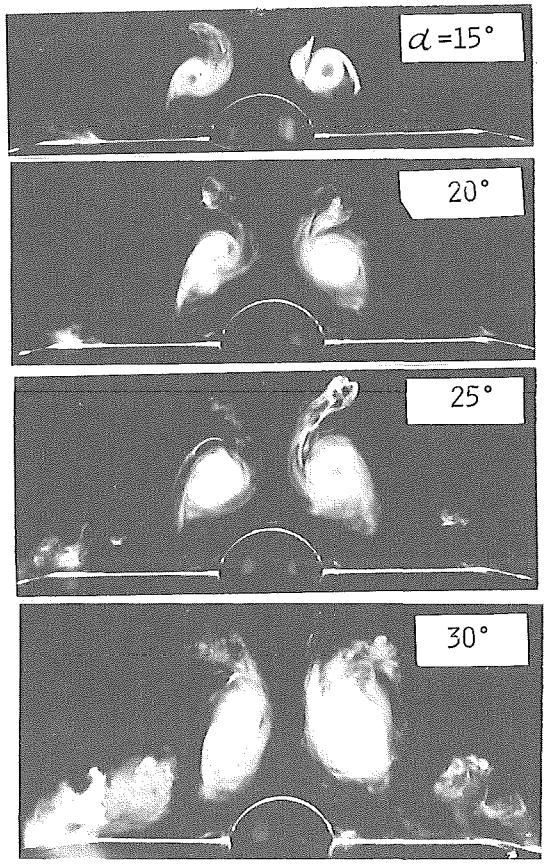

Fig.9 Vortex patterns in wing cross-plane with increasing alpha: 30° L.E. flap configuration.

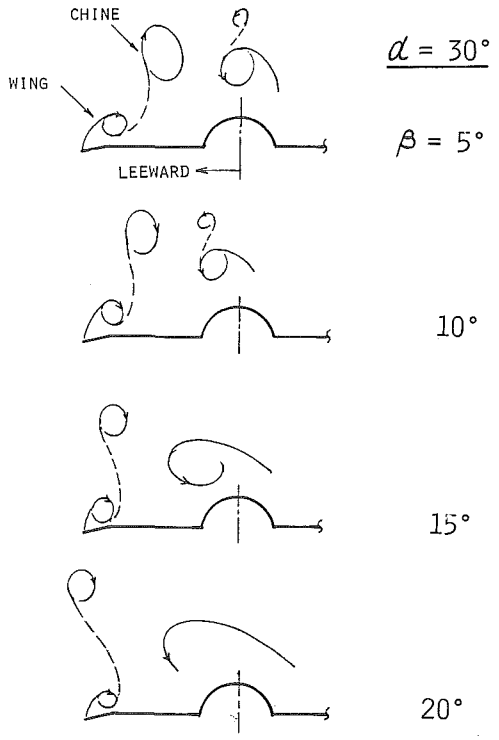

Fig.10 Vortex patterns in wing cross-plane with increasing side-slip; 30° deflected L.E. flaps.

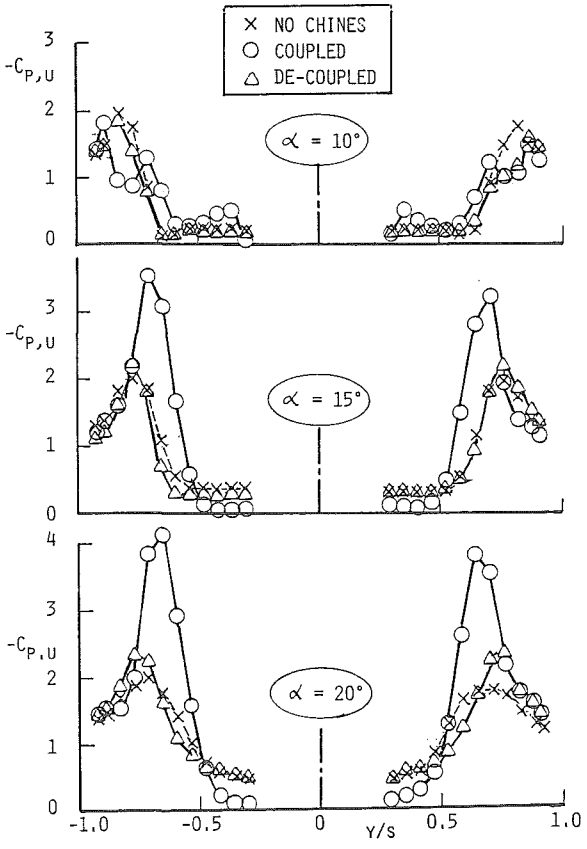

Fig.11,A Spanwise wing suction-pressure distributions with increasing alpha; comparison of no chines, coupled and de-coupled chines.

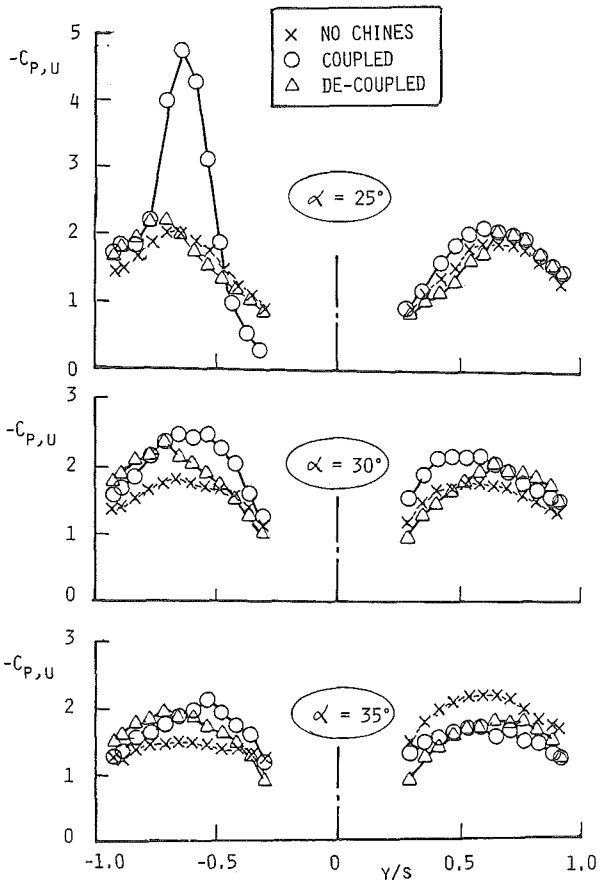

Fig.11,B Spanwise suction-pressure distributions with increasing alpha; compariosn of no-chines, coupled and de-coupled chines.

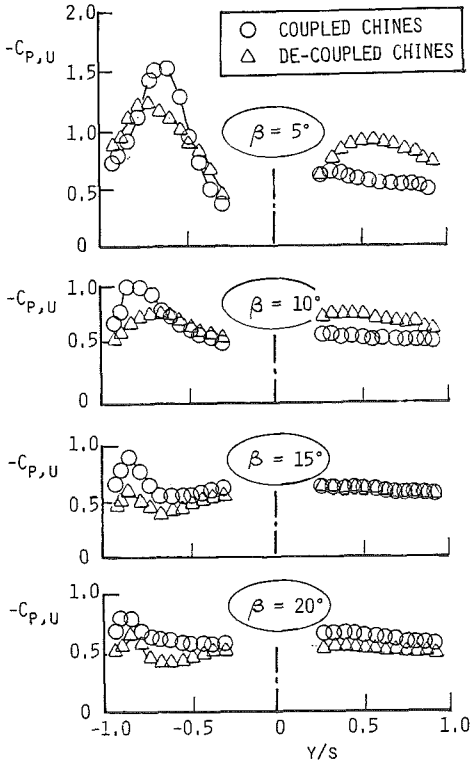

Fig.12 Spanwise wing suction-pressure distributions with increasing side-slip; coupled versus de-coupled chines.

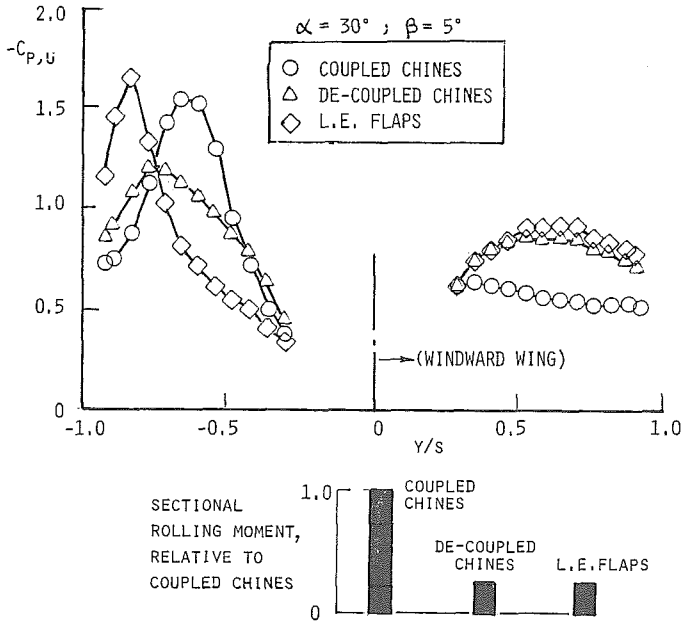

Fig.13 Spanwise wing suction-pressure distributions at side-slip; compariosn of coupled chines, de-coupled chines and 45° L.E. flaps.

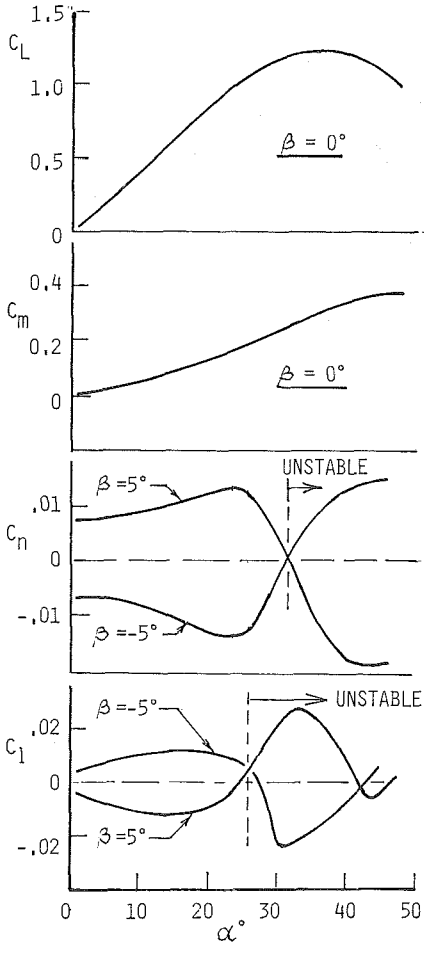

Fig.14 Lift and moment characteristics versus alpha; coupled chines.

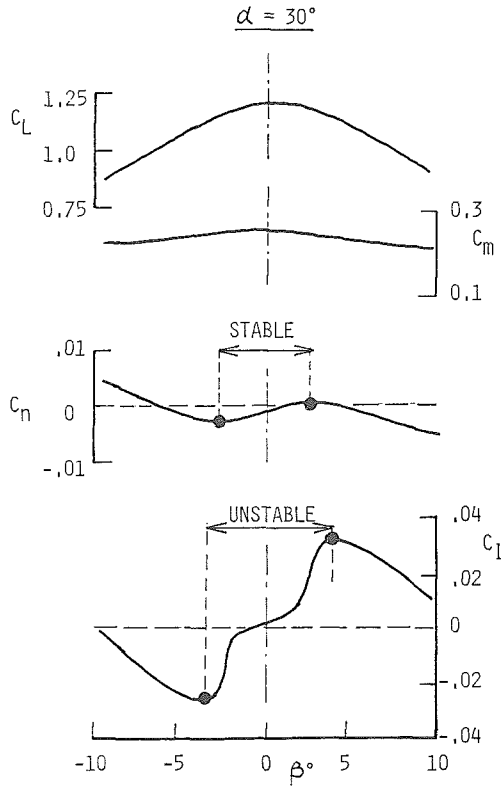

Fig.15 Lift and moment characteristics versus beta; coupled chines.

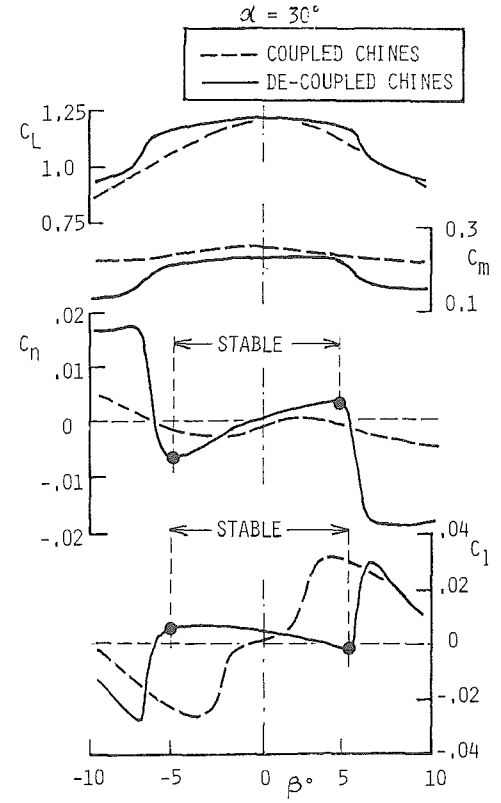

Fig.16 Lift and moment characteristics versus beta; comparison of coupled and de-coupled chines.

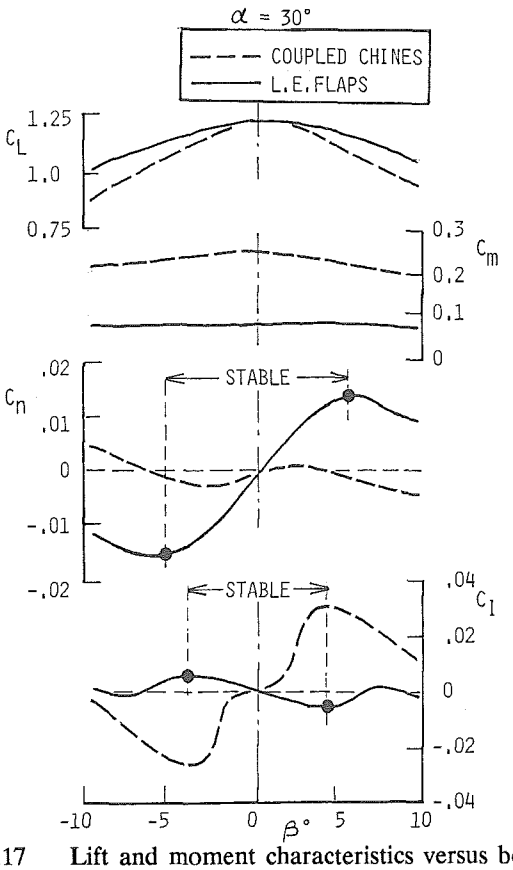

Fig.17 Lift and moment characteristics versus beta; comparison of coupled chines and 45° L.E. flaps.

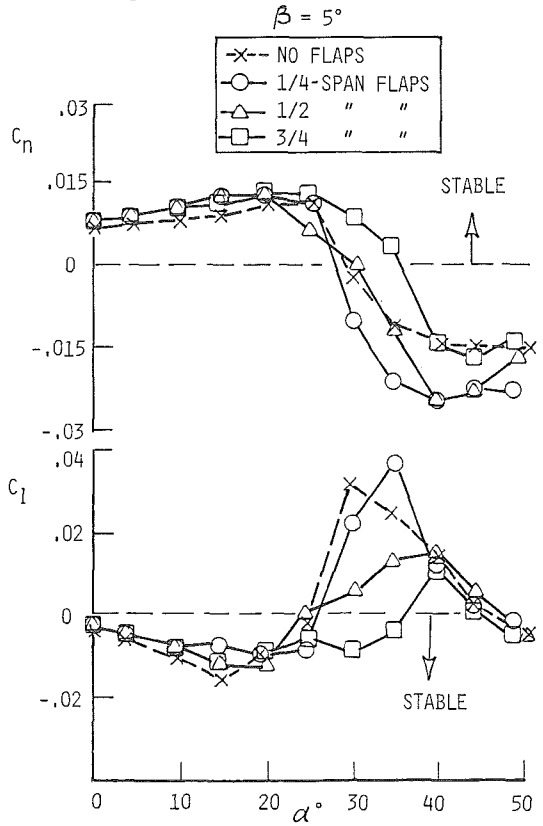

Fig.18 Directional and lateral stability characteristics versus alpha with varying L.E. flap span.

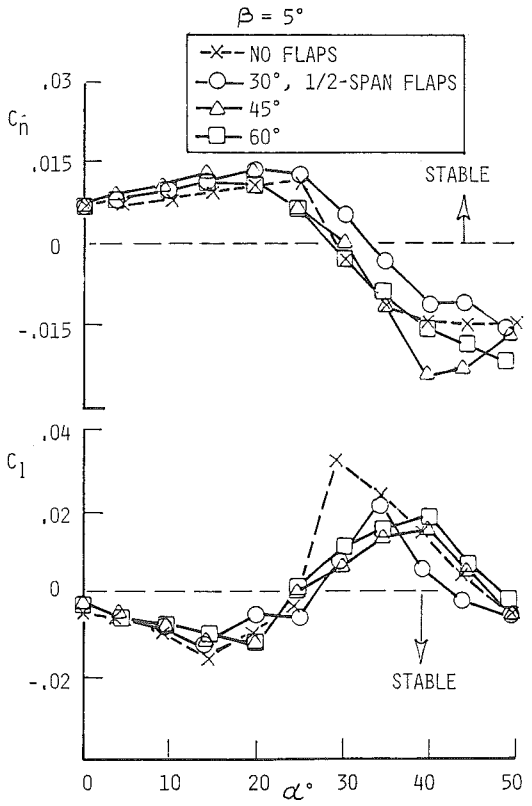

Fig.19 Directional and lateral stability characteristics versus alpha with varying L.E. flap deflection angle.

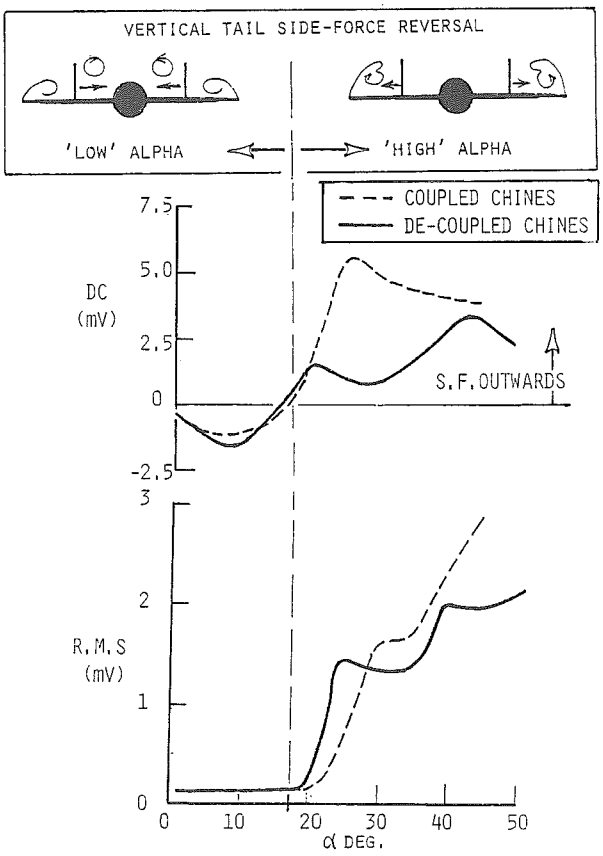

Fig.20 Right vertical-tail root bending output versus alpha; comparison of coupled and de-coupled chines.

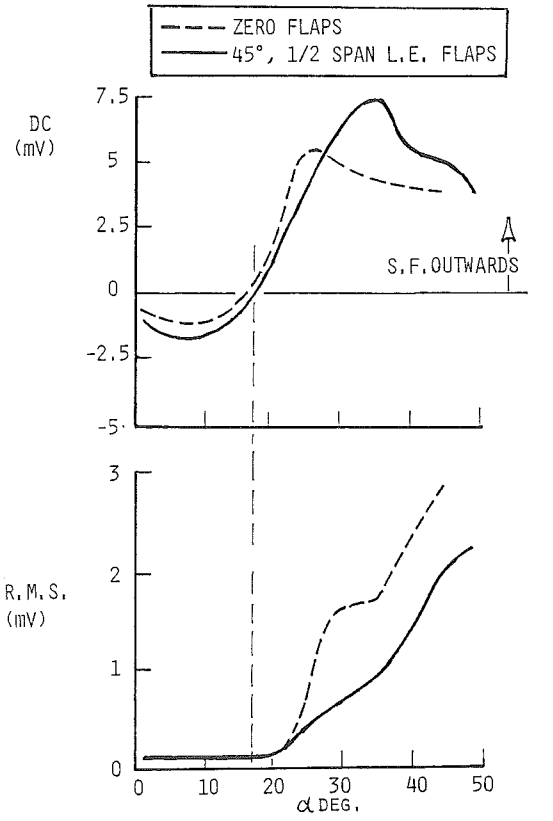

Fig.21 Right vertical-tail root bending output versus alpha; comparison of coupled chines and L.E. flaps.